Article

Structural and Spectroscopic Features of the Bixbyite-Type Yttrium Scandate Doped by Rare-Earth Ions

Elena Dobretsova *[ID], **Olimkhon Alimov, Denis Guryev** [ID], **Valery Voronov, Sergey Rusanov, Vitaly Kashin, Sergey Kutovoy, Viktor Vlasov, Lubov Badyanova, Ivan Novikov** [ID] **and Vladimir Tsvetkov**

Prokhorov General Physics Institute of the Russian Academy of Sciences, 119991 Moscow, Russia
* Correspondence: eadobr@kapella.gpi.ru

Abstract: Yttrium scandate crystal fiber has been obtained through laser-heated pedestal growth. The crystal belongs to a bixbyite crystal structure and crystallizes in $Ia\bar{3}$ space group. X-ray diffraction method shows a lattice parameter of a = 10.228(1) Å. Factor-group analysis of $YScO_3$ Raman spectra points to high degree of disorder in crystal structure of the new compound. Spectral-kinetic investigation of the crystal fibers doped by rare-earth ions points to the presence of two independent active optical centers of rare-earth ions. Moreover, the character of rare-earth impurities' distribution is independent on a rare-earth ionic radius size.

Keywords: yttrium scandate; bixbyite; laser-heated pedestal growth; X-ray diffraction; Raman spectroscopy; laser selective spectroscopy

1. Introduction

In recent years, there has been a global tendency to replace radio communication lines within satellite constellations, as well as between satellites and ground objects [1]. There is a fundamental problem of searching for an active laser medium for use in atmospheric and space optical communication systems (FSO). To organize space or long-range atmospheric optical communication, laser systems with high energy characteristics and, therefore, laser media that can withstand extreme optical, radiational and thermal loads are needed.

High melting rare-earth-doped sesquioxides can be promising materials for FSO applications. Due to the disordered crystal structure, rare-earth-doped mixed sesquioxides (such as yttrium scandate $YScO_3$) have inhomogeneously broadened spectral lines [2,3] which provides an advantage for its highly efficient pumping with modern diodes with low requirements for their thermal stabilization. Instead of the Czochralski method [4,5], we propose the use of the laser-heated pedestal method, which is more suitable for the growth of the high-melting crystals of good optical quality and small size required for use in equipment. In this approach, crystal synthesis is accompanied by high-temperature heating with laser radiation and subsequent rapid cooling.

Scandia (Sc_2O_3) and yttria (Y_2O_3) crystallize in a bixbyite structural type and have high thermal conductivity (two times more than yttrium aluminum garnet) [6] and a wide transparency window of 0.25 to 9.6 μm [7]. These properties are critically important for solid-state laser application. [3,8,9] Therefore, yttria and scandia may become alternative materials and replace YAG crystals in some applications. Ceramics based on rare-earth oxides [10] and mixed sesquioxides [11–16] are declared as excellent laser materials. Moreover, sesquioxides are advanced materials for application as white light emitting phosphors, [17,18] high effective luminescent materials, [19,20] rare-earth magnets, [21,22] optical recording and storage [23].

Yttrium scandate has a polymorphic nature. Its high-temperature modification [24,25], similar to yttria [26] and scandia [27], belongs to a bixbyite structural type with the space group $Ia\bar{3}$. The crystal structure includes one site of oxygen ion with local symmetry

C_1 (Wykoff position 48*e*) and two symmetrically independent sites of cations with local symmetry C_{3i} (Wykoff position 8*b*) and C_2 (Wykoff position 24*d*). The ionic radii of yttrium (0.9 Å), scandium (0.83 Å) and rare-earths are close, and the substitution of basic cations by rare-earth impurities does not require charge compensation and it is crystallochemically unforbidden.

Here we have synthesized and characterized the $YScO_3$ crystal fibers, pure and doped by 0.1 at. % Nd^{3+} and Tm^{3+} ions. Nd^{3+} and Tm^{3+} ion situate in different ends of lanthanoid group and have a maximal different ionic radius. Nd^{3+} belongs to large rare-earth ions while Tm^{3+} is a small ion. Moreover, Nd^{3+} is a Kramers ion with an odd number of electrons, and Tm^{3+} belongs to non-Kramers ions, with an even number of electrons. Therefore, Nd^{3+} and Tm^{3+} are maximally different ions and would presumably have different spectral behavior, which is related to the local structure of optically active centers. We have used selective laser spectroscopy methods, in which the luminescence spectra are recorded at selective excitation and, conversely, the excitation spectra are measured at selective detection. This approach allows us to trace local changes at included ion-activators. In this work, we have focused on studying the influence of rare-earth ion radius size on spectroscopic properties and the character of rare-earth impurities' distribution.

2. Results and Discussion

To grow the crystal fiber, high pure powders of scandium and yttrium oxides have been mixed in an agate mortar up to a homogeneous state. The mixture of Y_2O_3, Sc_2O_3 and RE_2O_3 (Tm_2O_3 or Nd_2O_3) was used as precursor to grow *RE*-doped crystal fibers. Then, the mixture has been transferred to a platinum crucible and annealed at a temperature of 1100 °C for 48 h. The powder rod of Y_2O_3-Sc_2O_3 composition has been obtained at the pressure of 20 MPa. The powder rod had length of 50 mm and diameter of 1 mm.

The rod was fixed vertically, and its tip was heated and melted at CO_2 laser irradiation. An yttria-stabilized zirconia (YSZ) crystal was used as a seed. It was dipped into the melt and raised slowly, pulling a crystal fiber with an approximately round cross-section from the melt. At a growth rate of about 80 mm/h, a $YScO_3$ crystal fiber with a diameter of 0.85 mm and length of 50 mm has been obtained.

The image in back-scattered electrons, the brightness of which depends on the average atomic number and the density of the substance, demonstrates the homogeneity of the crystal composition (Figure 1a). According to X-ray spectral analysis (SEM-EDS) the amounts of Sc and Y are almost equal and unchanging across the fiber (Figure 1b). Therefore, the crystal composition may be presented as $Y_{0.95}Sc_{1.05}O_3$, while taking into account three oxygen atoms per formula unit.

Structural characteristics of the crystal fiber, as well as powders of Y_2O_3 and Sc_2O_3 precursors, have been obtained with the X-ray phase analysis. The X-ray pattern of $YScO_3$ includes good narrow peaks that point to a high degree of crystallinity (Figure 1c). According to X-ray data, the $YScO_3$ crystal fiber is homogeneous and belongs to the bixbyite structural type (space group $Ia\bar{3}$), similar to yttrium and scandium sesquioxides (Figure 1c, insert). The lattice parameters of $YScO_3$, Y_2O_3 and Sc_2O_3 were obtained as *a* ($YScO_3$) = 10.228(1) Å, *a* (Y_2O_3) = 10.604(1) Å and *a* (Sc_2O_3) = 9.841(4) Å, respectively. Due to the low concentration of Nd^{3+} and Tm^{3+} ions in the $YScO_3$ host (about 0.1 at. %), *RE* impurity does not influence bixbyite-type crystal structure, phonon structure and crystal quality. XRD (Supplementary Materials Figure S1, Table S1) and Raman spectra (Figure S2) of the pure and rare-earth doped $YScO_3$ crystal fibers have been added as Supporting Information. Table 1 shows indexation of the most intensive peaks.
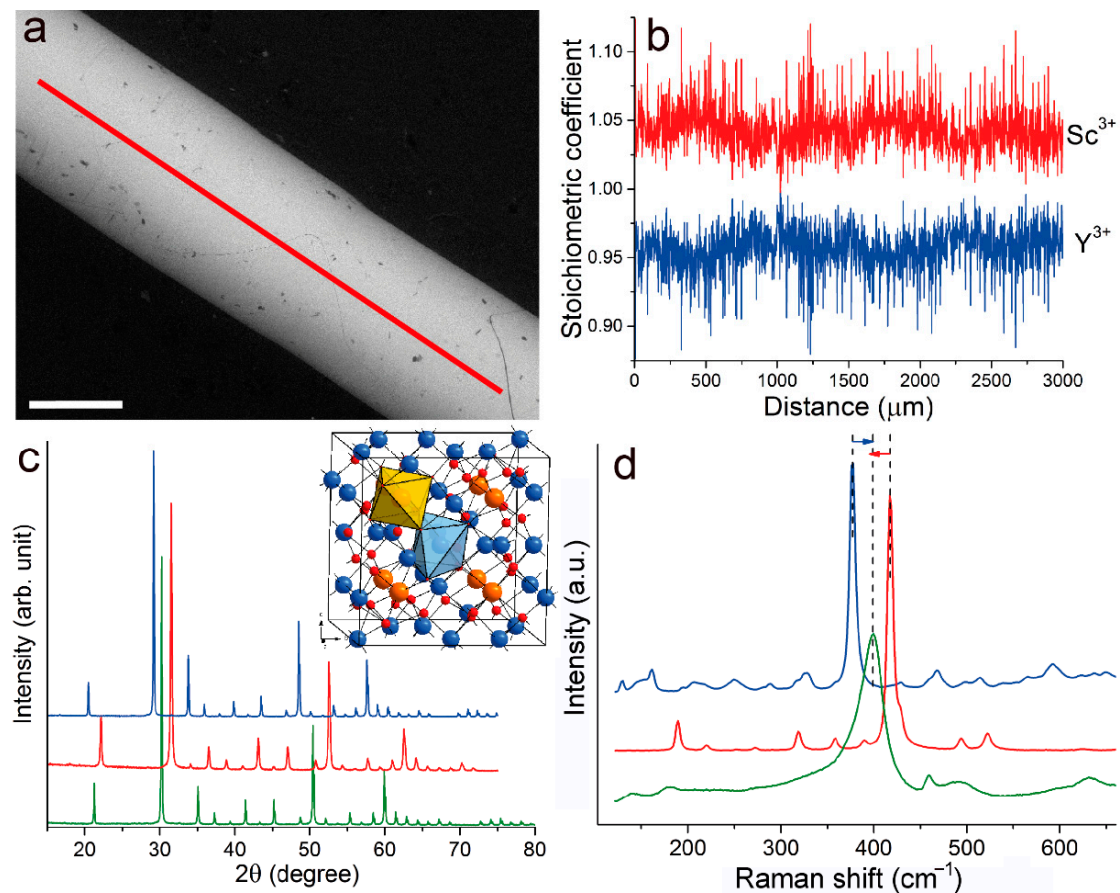
Figure 1. (**a**) An image of the $YScO_3$ crystal fiber captured in backscattered electron mode (BSE). A scalebar is 0.5 mm; (**b**) Stoichiometric coefficients of Y^{3+} (blue one) and Sc^{3+} (red one) ions calculated based on three oxygen atoms per formula unit; (**c**) The X-ray pattern of the $YScO_3$ crystal fiber (green one) and Y_2O_3 and Sc_2O_3 precursors (blue and red ones, respectively). Insert: bixbyite-type crystal structure of $YScO_3$. Symmetrically diverse MO_6 polyhedra both centered by statistically distributed Y^{3+} and Sc^{3+} ions are shown as orange (C_{3i} site) and blue (C_2 site); red balls are O atoms; (**d**) Raman spectra of Y_2O_3 and Sc_2O_3 precursors and $YScO_3$ crystal fiber (blue, red and green lines, respectively).

Table 1. Miller indices (*hkl*), interplanar distances *d*, Bragg angles 2θ and Bragg peak intensities *I* of the Y_2O_3, Sc_2O_3 and $YScO_3$ with a bixbyite-type structure.

			Y_2O_3; $a = 10.604(1)$ Å			Sc_2O_3; $a = 9.841(4)$ Å			$YScO_3$; $a = 10.228(1)$ Å		
Index	*hkl*	*m*	2θ	*d*	*I*	2θ	*d*	*I*	2θ	*d*	*I*
1	211	24	20.494	4.3302	13.90	22.139	4.0121	19.30	21.261	4.1756	13.54
2	222	8	29.162	3.0598	100.00	31.505	2.8374	100.00	30.246	2.9526	100.00
3	004	6	33.798	2.6500	21.90	36.53	2.4578	8.30	35.065	2.5570	18.45
4	411	24	35.918	2.4982	4.40	38.834	2.3171	3.50	37.268	2.4108	4.62
5	332	24	39.862	2.2597	4.70	43.121	2.0962	11.90	41.372	2.1806	8.36
6	341	24	43.51	2.0783	5.80	47.089	1.9284	8.60	45.166	2.0059	9.11
7	251	24	46.925	1.9347	1.70	50.814	1.7954	3.30	48.724	1.8674	3.27
8	044	12	48.556	1.8735	27.80	52.607	1.7383	39.10	50.432	1.8081	47.56
9	433	24	50.161	1.8172	1.30	54.344	1.6868	1.60	52.098	1.7541	2.14
10	611	24	53.245	1.7190	2.70	57.737	1.5955	4.10	55.324	1.6592	3.47
11	541	24	56.211	1.6351	2.10	61.002	1.5177	3.50	58.429	1.5782	4.54
12	622	24	57.657	1.5975	13.60	62.595	1.4828	14.20	59.942	1.5419	27.23
13	631	24	59.082	1.5623	2.70	64.166	1.4503	4.20	61.433	1.5081	6.56
14	444	8	60.478	1.5296	2.20	65.714	1.4198	1.20	62.903	1.4763	3.66
15	721	24	64.575	1.4421	1.60	70.255	1.3387	2.90	67.205	1.3919	3.08
16	008	6	71.123	1.3245	1.50				74.098	1.2785	4.70

The micro-Raman spectra have been obtained for Y_2O_3 and Sc_2O_3 powders and the $YScO_3$ crystal fiber (Figure 1d).

The unit cell of the bixbyite-type yttrium scandate includes 40 atoms (8 formula units). Therefore, factor-group analysis leads to the following distribution of the 120 phonon modes in the Brillouin zone point $\Gamma = 0$:

$$
\begin{aligned}
\Gamma = (3A_g + 3A_u + 3E_g + 3E_u + 9F_g + 9F_u)(C_1 \text{ local symmetry}) \\
+ \left(A_g + A_u + E_g + E_u + 5F_g + 5F_u\right)(C_2 \text{ local symmetry}) \\
+ \left(A_u + E_u + 3F_u\right)(C_{3i}\,(S_6\,)\text{ local symmetry})
\end{aligned}
\tag{1}
$$

After subtracting $1F_u$ of the acoustic modes there remain $16F_u$ of the infra-red active, $(4A_g + 4E_g + 14F_g)$ of the Raman-active and $(5A_u + 5E_u)$ of the optically inactive phonon modes. In the $Sc_2O_3 \rightarrow YScO_3 \rightarrow Y_2O_3$ series, we observed "mass effect" when vibrational modes are shifted to the range of lower frequencies with increasing cation mass. The spectral lines of yttrium scandate are broadened due to the presence of both Y^{3+} and Sc^{3+} cations in statistically equal structural positions. Due to partial overlap, a number of experimental lines are lower than predicted with factor-group analysis. Table 2 shows identification of the Raman-active modes [28].

Table 2. Raman-active modes in spectra of Y_2O_3, Sc_2O_3 and $YScO_3$; exp.—experimental, calc.—calculated.

Assignments [28]	Sc_2O_3, exp. [28]	Sc_2O_3, calc. [28]	Sc_2O_3	$YScO_3$	Y_2O_3, exp. [28]	Y_2O_3, calc. [28]	Y_2O_3
A_g	221	220	220	180	162	162	161
	391	351	358	-	-	306	318
	495	498	494	-	431	460	467
	623	593	-	590	-	553	542
E_g	273	273	273	-	194	198	194
	359	332	-	-	325	290	288
	430	416	429	400	-	366	358
	626	590	-	-	-	555	567
F_g	189	192	189	140	129	132	129
	202	199	-	180	138	138	152
	252	250	253	-	182	181	207
	319	306	-	-	235	234	217
	329	311	319	-	-	244	250
	359	341	358	-	325	288	288
	-	368	-	-	-	299	-
	391	386	390	-	-	338	327
	419	412	418	400	377	368	377
	-	472	-	460	-	416	429
	-	491	494	-	-	442	467
	523	536	522	495	469	495	499
	587	605	624	590	-	545	514
	669	646	670	630	592	581	592

Time-resolved luminescence excitation spectra of $Nd^{3+}:YScO_3$ have been obtained for $^4I_{9/2} \rightarrow {}^4F_{5/2} + {}^2H_{9/2}$ electro-dipole transitions in the Nd^{3+} ion at selective detection of 896 nm ($^4F_{3/2} \rightarrow {}^4F_{9/2}$ transition) at a temperature of 77 K (Figure 2a). Two intensive peaks are observed at 821.4 and 823.8 nm. The ratio of line intensities depends on delay in registration.
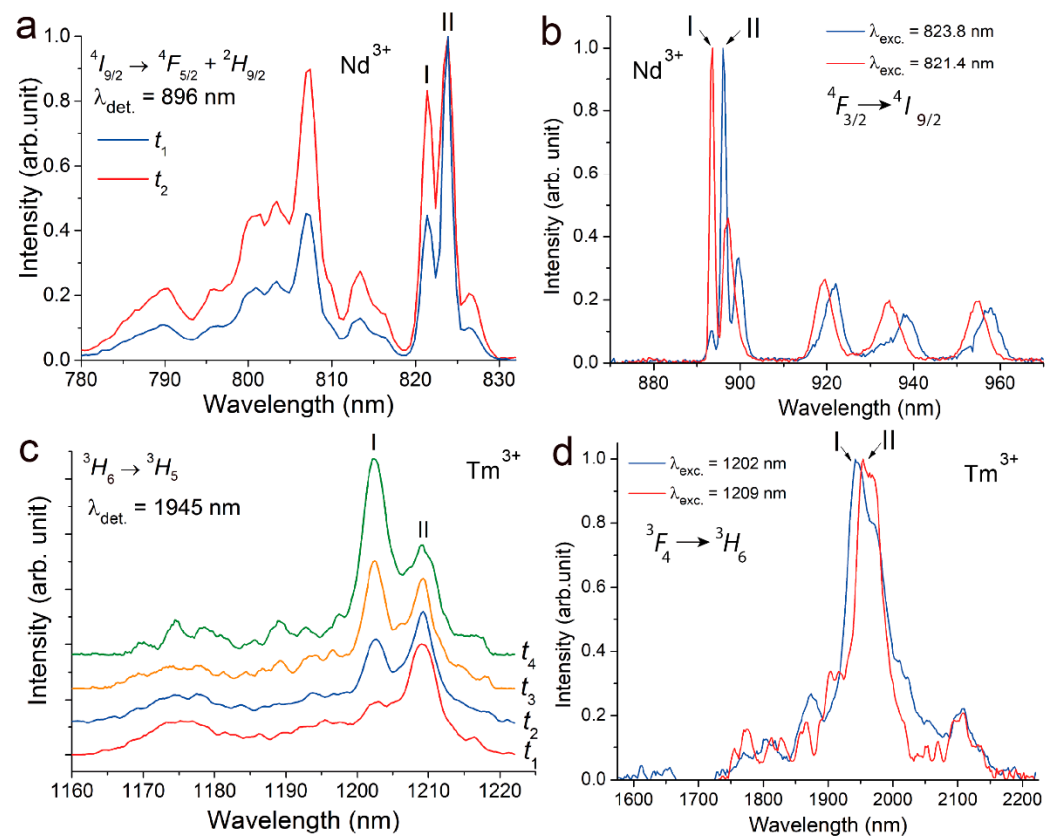
Figure 2. (**a**) Luminescence excitation spectra of $Nd^{3+}:YScO_3$ being obtained at a time delay of: $t_1 = 20$ µs; $t_2 = 254$ µs. (**b**) Luminescence spectra of $Nd^{3+}:YScO_3$ being obtained at excitation wavelength of 823.8 and 821.4 nm. (**c**) Luminescence excitation spectra of $Tm^{3+}:YScO_3$ being obtained at a time delay of: $t_1 = 0.6$ ms; $t_2 = 6$ ms; $t_3 = 10$ ms; $t_4 = 12$ ms. (**d**) Luminescence spectra of $Tm^{3+}:YScO_3$ being obtained at excitation wavelength of 1202 and 1209 nm. All measurements were accomplished at 77 K.

Figure 2b shows the luminescence emission spectra of Nd^{3+} ions being measured in the $^4F_{3/2} \to {}^4I_{9/2}$ electron transitions at 77 K. Nd^{3+} ions have been excited at 823.6 and 821.4 nm, which corresponds to a maximum of peaks being observed in luminescence excitation spectra.

Analysis of the spectra allows us to distinguish two independent optical centers of Nd^{3+} ions. The luminescence kinetics have been recorded on the $^3F_{3/2} \to {}^4I_{9/2}$ electron transition at two different excitation wavelengths (823.6 and 821.4 nm). In both cases, decay curves are described by exponential law with lifetimes of $\tau_1(77 \text{ K}) = 290$ µs (at 823.6 nm excitation) and $\tau_2(77 \text{ K}) = 250$ µs (at 821.4 nm excitation). The close lifetimes and relatively equal intensities of the spectral lines obtained from two different centers indicate the same C_2 symmetry in both cases. As is known [29], electro-dipole transitions are forbidden for rare-earth ion occupied centro-symmetric positions, in particular, the C_{3i} position in the bixbyite structure. The luminescence for these centers must be non-active. We assume that both of the centers have local symmetry of C_2. Probably, one of them forms as a result of the local substitution of the Y^{3+} cation by an Nd^{3+} ion, and another one is a result of the local substitution of the Sc^{3+} cation by an Nd^{3+} ion in the $YScO_3$ host.

The Tm^{3+} ion has the same behavior in $Tm^{3+}:YScO_3$. Luminescence excitation spectra of $Tm^{3+}:YScO_3$ have been obtained for of $^3H_6 \to {}^3H_5$ magneto-dipole transitions in the Tm^{3+} ion at selective detection of 1945 nm ($^3F_4 \to {}^3H_6$ transition) at a temperature of 77 K (Figure 2c). Two intensive peaks are observed at 1202.4 and 1209.4 nm. Ratio of line intensities depends on delay in registration in time-resolved spectra. This indicates the presence of two optical centers of Tm^{3+} ion with two different lifetimes.

Figure 2d shows luminescence spectra of Tm^{3+} ions being measured in the $^3F_4 \to {}^3H_6$ electron transition at selective excitation of 1202.4 and 1209.4 nm. The luminescence kinetics have been recorded on the $^3F_4 \to {}^4H_6$ electron transition at two different excitations of 1202.4 and 1209.4 nm. In both cases, decay curves are described by exponential law with lifetimes of τ_1(77 K) = 4.25 ms (at 1202.4 nm excitation) and τ_2(77 K) = 3.7 ms (at 1209.4 nm excitation). The close lifetimes and relatively equal intensities of the spectral lines obtained from two different centers indicate the same C_2 symmetry in both cases. One of Tm^{3+} optical center forms as a result of the local substitution of the Y^{3+} cation by a Tm^{3+} ion, and another one is a result of the local substitution of the Sc^{3+} cation by a Tm^{3+} ion in the $YScO_3$ host.

3. Materials and Methods

To grow the $YScO_3$ crystal fiber, the laser heated pedestal growth (LHPG) method has been used [25,30,31]. This approach allows us to synthesize crystal in the form of a fiber and to obtain high-melting materials and compounding with disordered crystal structure. To prepare $RE_2O_3 - Y_2O_3 - Sc_2O_3$ powder, preform scandium, yttrium and rare-earth (Nd^{3+} or Tm^{3+}) oxides (purity of more than 99.999%, Sigma Aldrich, Burlington, MA, USA) were well mixed in a stoichiometric proportion (of mole ratio $RE_2O_3/Y_2O_3/Sc_2O_3$ = 0.1:99.9:100) in an agate mortar to form a homogeneous mixture. The mole ratio of 1:1 was used to prepare undoped $Y_2O_3 - Sc_2O_3$ powder preform. Then, the mixture was transferred to a platinum crucible and annealed at 1100 °C for 48 h in an air atmosphere to exclude the presence of H_2O. The final powder mixture was pressed at 20 MPa to form a rod with about 1 mm diameter and 50 mm length.

Visualization and chemical composition analysis of the $YScO_3$ crystal fiber were carried out on the EVO 10 scanning electron microscope (Zeiss Microscopy GmbH, Jena, Germany). The samples were examined at an accelerating voltage of 20 kV with a working distance of 9.0 mm in low vacuum operation (EP = 50 Pa) using a LaB6 cathode.

To obtain SEM imaging of the sample, part of the crystal fiber was placed onto a carbon tape. The observations of the sample were carried out at a beam current of 85 pA. The images were captured in backscattered electron mode (BSE) to assess sample homogeneity (Figure 1a).

The semi-quantitative estimation of the main cation (Y^{3+} and Sc^{3+}) ratio was based on the data of the Smart METEK EDX spectrometer. Scanning was carried out in line-scan mode at a step of 2 μm and a beam current of 149 pA.

A part of the crystal fiber has been ground in an agate mortar and characterized with X-ray phase analysis. The X-ray pattern has been recorded on the Bruker D8 Discover A25 DaVinci Design diffractometer in the range of 2θ = 15–80° with a step of 0.02° and an exposition time of 1.0 s. The Siemens KFL X-ray tube with Cu $K\alpha$ (U = 40 kV, I = 40 mA, λ = 0.154 nm) irradiation has been used as the X-ray source. The spectra have been resolved with the EVA 2.1 software and identified with the PDF-2 2011 database. The TOPAS 4.2 software has been used to index spectral peaks and to determine lattice cell parameters.

Micro-Raman spectra of the $YScO_3$ crystal fiber and precursor (Y_2O_3 and Sc_2O_3) powders have been recorded on the EnSpectr R532 express analyzer equipped with the Olympus microscope (40× objective) at a laser excitation of 532 nm. The laser beam has been focused on a core of the fiber. Each spectrum has been obtained as the difference between the spectrum taken with the laser running and the dark spectrum. The subtraction of the first spectrum from the second one was carried out automatically using the EnSpectr Pro software. The final Raman spectra were obtained by averaging 20 runs acquired during the total time of 90 s (4.5 s for a run).

Spectral-kinetic characteristics of the Nd^{3+}- and Tm^{3+}-doped $YScO_3$ crystal fibers have been obtained with the selective spectroscopy method. Luminescence spectra have been recorded on the MDR–23 monochromator. The Hamamatsu R5108 и FEU-83 photomultipliers have been used as detectors. The LQ529B–LP 604 (Solar LS, Belarus) laser complex has been used as the excitation source.

4. Conclusions

A $YScO_3$ crystal fiber has been obtained through laser-heated pedestal growth (LHPG). According to X-ray spectral analysis (SEM-EDS), the amounts of Sc and Y are almost equal and unchanging across the fiber. The $YScO_3$ crystal fiber is homogeneous and belongs to the bixbyite structural type (space group $Ia\bar{3}$). The factor group analysis predicted 22 Raman-active phonon modes. However, due to partial overlap, a number of experimental lines are lower than predicted with factor-group analysis. Luminescence excitation and luminescence spectra of Tm^{3+}:$YScO_3$ and Nd^{3+}:$YScO_3$ show the presence of two active centers of the rare-earth ions in both cases. We suppose that one of rare-earth optical centers forms as a result of the local substitution of the Y^{3+} cation by an RE^{3+} ion, and another one is a result of the local substitution of the Sc^{3+} cation by an RE^{3+} ion in the $YScO_3$ host. Therefore, the nature of the inclusion of a rare-earth impurity into the $YScO_3$ bixbyite-type crystal structure does not depend on the ionic radius size of rare-earths.

References

1. Garlinska, M.; Pregowska, A.; Masztalerz, K.; Osial, M. From Mirrors to Free-Space Optical Communication—Historical Aspects in Data Transmission. *Future Internet* **2020**, *12*, 179. [CrossRef]
2. Liu, W.; Lu, D.; Pan, S.; Xu, M.; Hang, Y.; Yu, H.; Zhang, H.; Wang, J. Ligand Engineering for Broadening Infrared Luminescence of Kramers Ytterbium Ions in Disordered Sesquioxides. *Cryst. Growth Des.* **2019**, *19*, 3704–3713. [CrossRef]
3. Liu, W.; Lu, D.; Guo, R.; Wu, K.; Pan, S.; Hang, Y.; Sun, D.; Yu, H.; Zhang, H.; Wang, J. Broadening of the Fluorescence Spectra of Sesquioxide Crystals for Ultrafast Lasers. *Cryst. Growth Des.* **2020**, *20*, 4678–4685. [CrossRef]
4. Suzuki, A.; Kalusniak, S.; Tanaka, H.; Brützam, M.; Ganschow, S.; Tokurakawa, M.; Kränkel, C. Spectroscopy and 2.1 μm Laser Operation of Czochralski-Grown Tm^{3+}:$YScO_3$ Crystals. *Opt. Express* **2022**, *30*, 42762–42771. [CrossRef]
5. Kränkel, C.; Uvarova, A.; Haurat, É.; Hülshoff, L.; Brützam, M.; Guguschev, C.; Kalusniak, S.; Klimm, D. Czochralski Growth of Mixed Cubic Sesquioxide Crystals in the Ternary System Lu_2O_3-Sc_2O_3-Y_2O_3. *Acta Crystallogr. B Struct. Sci. Cryst. Eng. Mater.* **2021**, *77*, 550–558. [CrossRef]
6. Klein, P.H.; Croft, W.J. Thermal Conductivity, Diffusivity, and Expansion of Y_2O_3, $Y_3Al_5O_{12}$, and LaF_3 in the Range 77–300° K. *J Appl. Phys.* **1967**, *38*, 1603. [CrossRef]
7. Nigara, Y. Measurement of the Optical Constants of Yttrium Oxide. *Jpn. J. Appl. Phys.* **1968**, *7*, 404. [CrossRef]
8. Heuer, A.M.; von Brunn, P.; Huber, G.; Kränkel, C. Dy^{3+}:Lu_2O_3 as a Novel Crystalline Oxide for Mid-Infrared Laser Applications. *Opt. Mater. Express* **2018**, *8*, 3447–3455. [CrossRef]
9. Tokurakawa, M.; Shirakawa, A.; Ueda, K.; Peters, R.; Fredrich-Thornton, S.T.; Petermann, K.; Huber, G. Ultrashort Pulse Generation from Diode Pumped Mode-Locked Yb^{3+}:Sesquioxide Single Crystal Lasers. *Opt. Express* **2011**, *19*, 2904–2909. [CrossRef]

10. Loiko, P.; Koopmann, P.; Mateos, X.; Serres, J.M.; Jambunathan, V.; Lucianetti, A.; Mocek, T.; Aguilo, M.; Diaz, F.; Griebner, U.; et al. Highly Efficient, Compact Tm^{3+}: RE_2O_3 (RE = Y, Lu, Sc) Sesquioxide Lasers Based on Thermal Guiding. *IEEE J. Sel. Top. Quantum Electron.* **2018**, *24*, 1600713. [CrossRef]

11. Li, D.; Kong, L.; Xu, X.; Liu, P.; Xie, G.; Zhang, J.; Xu, J. Spectroscopy and Mode-Locking Laser Operation of $Tm:LuYO_3$ Mixed Sesquioxide Ceramic. *Opt. Express* **2019**, *27*, 24416–24425. [CrossRef] [PubMed]

12. Hao, Z.; Zhang, L.; Wang, Y.; Wu, H.; Pan, G.-H.; Wu, H.; Zhang, X.; Zhao, D.; Zhang, J. 11 W Continuous-Wave Laser Operation at 209 μm in $Tm:Lu_{1.6}Sc_{0.4}O_3$ Mixed Sesquioxide Ceramics Pumped by a 796 nm Laser Diode. *Opt. Mater. Express* **2018**, *8*, 3615–3621. [CrossRef]

13. Pirri, A.; Patrizi, B.; Maksimov, R.N.; Shitov, V.A.; Osipov, V.V.; Vannini, M.; Toci, G. Spectroscopic Investigation and Laser Behaviour of Yb-Doped Laser Ceramics Based on Mixed Crystalline Structure ($Sc_xY_{1-x})_2O_3$. *Ceram. Int.* **2021**, *47*, 29483–29489. [CrossRef]

14. Toci, G.; Pirri, A.; Patrizi, B.; Maksimov, R.N.; Osipov, V.V.; Shitov, V.A.; Yurovskikh, A.S.; Vannini, M. High Efficiency Emission of a Laser Based on Yb-Doped $(Lu,Y)_2O_3$ Ceramics. *Opt. Mater.* **2018**, *83*, 182–186. [CrossRef]

15. Pirri, A.; Maksimov, R.N.; Shitov, V.A.; Osipov, V.V.; Sani, E.; Patrizi, B.; Vannini, M.; Toci, G. Continuously Tuned ($Tm_{0.050}Sc_{0.252}Y_{0.698})_2O_3$ Ceramic Laser with Emission Peak at 2076 nm. *J. Alloys Compd.* **2022**, *889*, 161585. [CrossRef]

16. Pirri, A.; Maksimov, R.N.; Li, J.; Vannini, M.; Toci, G. Achievements and Future Perspectives of the Trivalent Thulium-Ion-Doped Mixed-Sesquioxide Ceramics for Laser Applications. *Materials* **2022**, *15*, 2084. [CrossRef]

17. Reenabati Devi, K.; Dorendrajit Singh, S.; David Singh, T. Photoluminescence Properties of White Light Emitting $La_2O_3:Dy^{3+}$ Nanocrystals. *Indian J. Phys.* **2018**, *92*, 725–730. [CrossRef]

18. Antoinette, M.M.; Israel, S.; Berchmans, J.L.; Manoj, G.J. Enhanced Photoluminescence and Charge Density Studies of Novel ($Sm_{1-x}Gd_x)_2O_3$ Nanophosphors for WLED Applications. *J. Mater. Sci. Mater. Electron.* **2018**, *29*, 19368–19381. [CrossRef]

19. Barrera, E.W.; Cascales, C.; Pujol, M.C.; Park, K.H.; Choi, S.B.; Rotermund, F.; Carvajal, J.J.; Mateos, X.; Aguiló, M.; Díaz, F. Synthesis of $Tm:Lu_2O_3$ Nanocrystals for Phosphor Blue Applications. *Phys. Procedia* **2010**, *8*, 142–150. [CrossRef]

20. Kumar, A.; Tiwari, S.P.; Kumar, K.; Rai, V.K. Structural and Optical Properties of Thermal Decomposition Assisted $Gd_2O_3:Ho^{3+}/Yb^{3+}$ Upconversion Phosphor Annealed at Different Temperatures. *Spectrochim. Acta A Mol. Biomol. Spectrosc.* **2016**, *167*, 134–141. [CrossRef]

21. El-Kelany, K.E.; Ravoux, C.; Desmarais, J.K.; Cortona, P.; Pan, Y.; Tse, J.S.; Erba, A. Spin Localization, Magnetic Ordering, and Electronic Properties of Strongly Correlated Ln_2O_3 Sesquioxides (Ln=La, Ce, Pr, Nd). *Phys. Rev. B* **2018**, *97*, 245118. [CrossRef]

22. Tseng, K.P.; Yang, Q.; McCormack, S.J.; Kriven, W.M. High-Entropy, Phase-Constrained, Lanthanide Sesquioxide. *J. Am. Ceram. Soc.* **2020**, *103*, 569–576. [CrossRef]

23. Balabanov, S.; Demidova, K.; Filofeev, S.; Ivanov, M.; Kuznetsov, D.; Li, J.; Permin, D.; Rostokina, E. Influence of Lanthanum Concentration on Microstructure of ($Ho_{1-x}La_x)_2O_3$ Magneto-Optical Ceramics. *Phys. Status Solidi B Basic Res.* **2020**, *257*, 1900500. [CrossRef]

24. Clark, J.B.; Richter, P.W.; Du Toit, L. High-Pressure Synthesis of $YScO_3$, $HoScO_3$, $ErScO_3$, and $TmScO_3$, and a Reevaluation of the Lattice Constants of the Rare Earth Scandates. *J. Solid State Chem.* **1978**, *23*, 129–134. [CrossRef]

25. Alimov, O.; Dobretsova, E.; Guryev, D.; Kashin, V.; Kiriukhina, G.; Kutovoi, S.; Rusanov, S.; Simonov, S.; Tsvetkov, V.; Vlasov, V.; et al. Growth and Characterization of Neodymium-Doped Yttrium Scandate Crystal Fiber with a Bixbyite-Type Crystal Structure. *Cryst. Growth Des.* **2020**, *20*, 4593–4599. [CrossRef]

26. Hanic, F.; Hartmanová, M.; Knab, G.G.; Urusovskaya, A.A.; Bagdasarov, K.S. Real Structure of Undoped Y_2O_3 Single Crystals. *Acta Crystallogr. Sect. B* **1984**, *40*, 76–82. [CrossRef]

27. Geller, S.; Romo, P.; Remeika, J.P. Refinement of the Structure of Scandium Sesquioxide. *Zeitschrift Kristallographie New Cryst. Struct.* **1967**, *124*, 136–142. [CrossRef]

28. Abrashev, M.V.; Todorov, N.D.; Geshev, J. Raman Spectra of R_2O_3 (R—Rare Earth) Sesquioxides with C-Type Bixbyite Crystal Structure: A Comparative Study. *J. Appl. Phys.* **2014**, *116*, 103508. [CrossRef]

29. Kaminskii, A.A. *Crystalline Lasers: Physical Processes and Operating Schemes*; CRC Press: Boca Raton, FL, USA, 2020; ISBN 9781003067962.

30. Feigelson, R.S. Pulling Optical Fibers. *J. Cryst. Growth* **1986**, *79*, 669–680. [CrossRef]

31. Bufetova, G.A.; Kashin, V.V.; Nikolaev, D.A.; Rusanov, S.Y.; Seregin, V.F.; Tsvetkov, V.B.; Shcherbakov, I.A.; Yakovlev, A.A. Neodymium-Doped Graded-Index Single-Crystal Fibre Lasers. *Quantum Electron.* **2006**, *36*, 616. [CrossRef]